ELSEVIER

Journal of Chromatography A, 954 (2002) 181–190

JOURNAL OF CHROMATOGRAPHY A

www.elsevier.com/locate/chroma

Temperature effects on the retention of *n*-alkanes and arenes in helium–squalane gas–liquid chromatography Experiment and molecular simulation

Collin D. Wick[a], J. Ilja Siepmann[a,*], Wendy L. Klotz[b], Mark R. Schure[b]

[a]*Departments of Chemistry and of Chemical Engineering and Materials Science, University of Minnesota, 207 Pleasant Street SE, Minneapolis, MN 55455, USA*

[b]*Theoretical Separation Science Laboratory, Rohm and Haas Company, 727 Norristown Road, P.O. Box 0904, Spring House, PA 19477, USA*

Received 5 December 2001; received in revised form 13 February 2002; accepted 13 February 2002

Abstract

Experiments and molecular simulations were carried out to study temperature effects (in the range of 323 to 383 K) on the absolute and relative retention of *n*-hexane, *n*-heptane, *n*-octane, benzene, toluene and the three xylene isomers in gas–liquid chromatography. Helium and squalane were used as the carrier gas and retentive phase, respectively. Both the experiments and the simulations show a markedly different temperature dependence of the retention for the *n*-alkanes compared to the arenes. For example, over the 60 K temperature range studied, the Kovats retention index of benzene is found to increase by about 16 or 18±10 retention index units determined from the experiments or simulations, respectively. For toluene and the xylenes, the experimentally measured increases are similar in magnitude and range from 14 to 17 retention index units for *m*-xylene to *o*-xylene. The molecular simulation data provide an independent method of obtaining the transfer enthalpies and entropies. The change in retention indices is shown to be the result of the larger entropic penalty and the larger heat capacity for the transfer of the alkane molecules. © 2002 Published by Elsevier Science B.V.

Keywords: Thermodynamic parameters; Temperature effects; Retention indices; Mathematical modelling; Computer simulation; Alkanes; Benzene; Toluene; Xylenes; Helium; Squalane

1. Introduction

Gas–liquid chromatography (GC) is often the method of choice for the separation of volatile compounds [1–3] with subsequent identification by retention time, retention index, or by mass spectrometry. Compound identification by retention time is flow-rate, phase thickness, and temperature sensitive amongst other problems and is rarely used except under the most limited of conditions. The retention index system [4–6] has been shown to be much better suited for compound identification within a limited set of compounds but still has a minor temperature dependence [1–3,6–11]. This is not a problem for compound identification under the best of conditions, but can be a burden when the index is not available at the temperature chosen for GC method development, or when temperature extrapolation of the index is not possible.

*Corresponding author. Tel.: +1-612-624-1844.

E-mail address: siepmann@chem.umn.edu (J.I. Siepmann).

0021-9673/02/$ – see front matter
PII: S0021-9673(02)00171-1

The Kovats retention index of a specific solute, I_x, can be calculated directly from partition coefficients such that:

$$I_x = 100n + 100 \cdot \left[\frac{\log (K_x/K_n)}{\log (K_{n+1}/K_n)} \right] \quad (1)$$

where K_x, K_n and K_{n+1} are the partition coefficients of the solute x and the n-alkanes (with n and $n+1$ carbons) that elute just before and after (or together with) solute x. The experimental retention time, t_r, can be related to the partition coefficient, K:

$$\phi K = \frac{t_r}{t_0} - 1 \quad (2)$$

where ϕ and t_0 are the phase ratio and void time (elution time of an unretained compound), respectively. The phase ratio is the ratio of stationary phase volume to mobile phase volume. Thus, this system offers a powerful, yet very simple, characterization of relative retention [6].

The empirical characterization of the temperature dependence of the retention index has been reported in a number of studies [6–11]. These studies incorporate thermodynamic models of retention into the retention index equation. Since the retention index system is entirely thermodynamic in origin [9], small departures from temperature independent behavior are typically explained through the temperature dependence of the individual enthalpic and entropic terms which make up the retention index equation.

Thermodynamic studies performed by chromatographic-based thermodynamic investigations [12] have not revealed the molecular origins of this temperature dependence. This is mostly due to the fact that molecular models of retention can not be constructed using only thermodynamic data [13].

Although a basic understanding of the governing principles of retention exist for GC, there is an incomplete understanding of how changes in physical conditions affect relative retention. For the case of partitioning of non-polar solutes between a vapor phase and a non-polar solvent, it is well known that the Gibbs free energies for the transfer from the vapor phase to the liquid phase increase with increasing temperature, but may do so at different rates [12]. While the use of experiment is often the best method to get high confidence measurements, molecular simulation can aid significantly in determining the origins of these experimentally-observed effects.

This can only be the case, though, if the simulation results are accurate enough to closely coincide with experimental measurements. Understanding the origins of temperature-dependent retention indices would allow for a more solid understanding of the overall retention process and could be very useful in further optimizing the GC experiment.

Here we describe an investigation which includes both experimental and computational approaches toward exhaustively studying the temperature effect on the retention indices of benzene and toluene. Using simulation, we can show in molecular detail how the temperature dependence arises and how this information can be used to further guide experimental insight into the chromatographic process.

2. Experimental details

All GC experiments were conducted with a Hewlett-Packard (Wilmington, DE, USA) model 6890 gas chromatograph equipped with a split–splitless injector. The detector utilized for these studies was a Hewlett-Packard mass selective detector model 5973. The data system was a Hewlett-Packard Kayak XA 500 MHz personal computer with MSD Productivity ChemStation software. Retention index experiments were carried out on a squalane column (30 m$\times$0.25 mm I.D., 0.25 μm film thickness) from Restek (Bellefonte, PA, USA), model 57529, for which the support material is completely deactivated prior to coating the squalane on the column. The carrier gas was helium at a flow-rate of 1 ml min^{-1}, and injections were performed in the split mode at a split ratio of 50:1. The first peak in the chromatograms was used to estimate the void time. The origin of this peak is dissolved air, as determined by the mass spectrometer detector. The variation in the void time was very small over the entire temperature range studied.

The retention index is calculated from experimental data according to the well-known formula [2,6]:

$$I_x = 100n + 100 \cdot \left[\frac{\log (t'_x/t'_n)}{\log (t'_{n+1}/t'_n)} \right] \quad (3)$$

The terms t'_x, t'_n and t'_{n+1} are the void-time corrected retention times of the analyte of interest, of the largest *n*-alkane with a retention time less than or equal to the analyte molecule, and of the next-higher *n*-alkane with a retention time larger than, or equal to, the analyte, respectively.

All analyte molecules (*n*-hexane to *n*-nonane, benzene, toluene and the three xylene isomers) were obtained from Aldrich (Milwaukee, WI, USA) and were used at a concentration of 500 μg g^{-1} in acetone solvent. The *n*-alkane and arene mixtures were injected separately. The oven temperature range was increased in 10 K increments from 323 to 383 K. The upper temperature experiments showed some noise that is indicative of column bleed. Hence, we have limited the measurements to 383 K or less. The recommended maximum temperature for a squalane column is 373 K [1].

3. Molecular models

The united-atom version of the transferable potentials for phase equilibria (TraPPE–UA) force field utilizes single interaction centers located on carbon atomic sites to mimic the interactions of CH_x groups (with $0 \leq x \leq 4$) in saturated and unsaturated hydrocarbons [14–16]. In the original version of the TraPPE–UA force field for alkanes and arenes, the non-bonded interactions of pseudoatoms are described solely by Lennard–Jones (LJ) interactions:

$$u_{\mathrm{LJ}}(r_{ij}) = 4\epsilon_{ij} \cdot \left[\left(\frac{\sigma_{ij}}{r_{ij}} \right)^{12} - \left(\frac{\sigma_{ij}}{r_{ij}} \right)^{6} \right] \tag{4}$$

where r_{ij}, ϵ_{ij} and σ_{ij} are the separation, LJ well depth and LJ diameter, respectively, for the pseudo-atoms *i* and *j*. These LJ potentials are effective potentials that describe overlap and dispersive interactions [17]. For unlike LJ interactions, the standard Lorentz–Berthelot combining rules are used [17], as follows:

$$\sigma_{ij} = \frac{\sigma_{ii} + \sigma_{jj}}{2} \qquad \epsilon_{ij} = \sqrt{\epsilon_{ii}\epsilon_{jj}} \tag{5}$$

For linear and branched alkanes, the strategy to rely solely on Lennard–Jones potentials to describe the non-bonded interactions was shown to yield highly satisfactory descriptions of the phase equilibria for neat and multicomponent systems, as well as of transfer properties [14,15,18–20]. The same can not be said for the description of the arenes for which slightly larger discrepancies with the experimental results were already observed for the neat phases [16]. Furthermore, the phase equilibria for alkane–arene mixture showed significant deviations from the experimental results [16,21]. In particular, with respect to the prediction of relative retention times in GC, it was found that the original TraPPE–UA description of the arenes yielded alkane–aromatic interactions that were too favorable, and the retention indices for benzene and toluene were about 38 and 30 units higher, respectively, than their experimental counterparts [21]. Apparently, when the interactions of the arenes are solely described by effective Lennard–Jones potentials, i.e. lumping both the attractive dispersive and quadrupolar interactions into an r^{-6} tail, then the unlike interactions between alkanes and arenes are too favorable. The obvious solution is to add separate quadrupolar interactions to the arenes and to re-fit their Lennard–Jones parameters. A similar strategy was already used successfully to determine a force field for carbon dioxide that is also very accurate for mixtures with alkanes [22].

For consistency with the other parts of the TraPPE force field, the quadrupolar interactions of an arene ring were described using three partial charges (instead of a point quadrupole) and the Coulomb potential:

$$u_{qq}(r_{ij}) = \frac{q_i q_j}{4\pi\epsilon_0 r_{ij}} \tag{6}$$

where q_i and q_j are the partial charges for sites *i* and *j*, respectively. For the new TraPPE–UA representation of the arenes, a positive partial charge ($q_{\mathrm{center}} = +2.42$ e) is placed at the center of the ring, and two negative partial charges representing the π-electron clouds are placed at a distance of 0.785 Å from the ring center and on a line perpendicular to the arene plane. The distance was obtained from an electronic structure calculation for benzene [23] and magnitudes of the partial charge were chosen to reproduce the quadrupole moment of benzene [24] and are similar to a previous benzene force field [25]. Once the partial charges are set, the Lennard–Jones parameters (well depth and diameter) for the aro-

matic CH united atom need to be re-fit from calculations of the vapor–liquid equilibria of benzene, and thereafter the parameters for the aromatic link to side chains can be determined from calculations for toluene.

The non-bonded interaction parameters for both the original and the new TraPPE–UA models are listed in Table 1. It can be observed that the new LJ diameter for the CH(arom) is slightly larger than the original one. The larger diameter is needed to off-set the enhanced ordering (and higher density) that is caused by the inclusion of the quadrupolar interactions. Whereas the LJ well depth for the CH(arom) site is now about 5% smaller to off-set the contribution of the quadrupolar interactions to the cohesive energy and heat of vaporization. The parameters for the R–C(arom) linker did not need to be updated because using the original R–C(arom) site in combination with the new CH(arom) sites and the same quadrupolar sites as for benzene yielded a vapor–liquid coexistence curve (VLCC) for toluene that agrees to within the statistical uncertainties with the experimental results. It should be noted that the R–C(arom) site is shielded by the methyl group and two CH(arom) sites, thus the calculated properties are less sensitive to changes in the parameters for the R–C(arom) site. For all simulations, the LJ interactions were truncated at 14 Å, and analytic tail corrections for the energy, pressure and chemical potential were employed [26]. A molecule-based truncation at 14 Å was also used for the quadrupolar interactions.

The description of the bonded parameters was retained from the original TraPPE–UA model [14–16]. Benzene and toluene are kept rigid, with a bond length of 1.40 Å for the (CH)–(CH) bonds and a bond angle of 120° for the arene rings. All (CH_x)–(CH_y) single bonds are fixed at 1.54 Å, but bond bending and dihedral motions are allowed for the saturated alkanes (the squalane solvent and the alkane solutes) [14,15]. The torsional flexibility of the benzene ring [27] and the environmental dependence of chemical bond lengths (e.g. the carbon–carbon bond length in *o*-xylene differ by about 0.02 Å) [28,29] are neglected in the TraPPE–UA model to achieve a simple and transferable force field and to improve the sampling efficiency.

Table 1
Comparison of old and new non-bonded parameters for arenes

Site	New model			Old model [16]	
	σ (Å)	ϵ/k_B (K)	q (K)	σ (Å)	ϵ/k_B (K)
CH(arom)	3.74	48	0	3.695	50.5
Center Site	0	0	2.42	–	–
Pi Site	0	0	−1.21	–	–
R–C(arom)	3.88	21	0	3.88	21
CH_3	3.75	98	0	3.75	98

For the refitting of the LJ parameters, the VLCCs for benzene and toluene were calculated following the usual approach, i.e. using configurational-bias Monte Carlo (CBMC) [14,30,31] in the constant-volume Gibbs ensemble [32–34]. The systems consisted of either 300 benzene or 300 toluene molecules, and the production runs varied from 50 000 Monte Carlo cycles at the lower temperatures to 100 000 Monte Carlo cycles at the higher temperatures. Other details of the VLCC simulations were the same as in previous work [16].

The vapor–liquid coexistence densities and saturated vapor pressures obtained for the new benzene and toluene models are compared to the experimental data [35] in Figs. 1 and 2, and the critical parameters and boiling points are listed in Table 2. The new benzene and toluene models appear to yield a satisfactory description of the saturated liquid densities and critical parameters, similar to the results obtained for the original benzene and toluene force field [16]. However, a significant improvement over the original model is evident for the saturated vapor pressures and the normal boiling temperatures. Although the saturated vapor pressures remain above the experimental values and the calculated boiling temperatures are a few degrees too low, these deviations are now much more consistent with the deviations observed for the TraPPE–UA model for the saturated alkanes [14,15], which should allow for more accurate predictions of the relative thermodynamic properties in alkane–arene mixtures. These small deviations from experiment can be attributed to the united-atom representation that does not yield an exact description of the molecular shape [36]. However, use of the more accurate explicit-hydrogen models [36] leads to an increase in computer time of about a factor of 5.

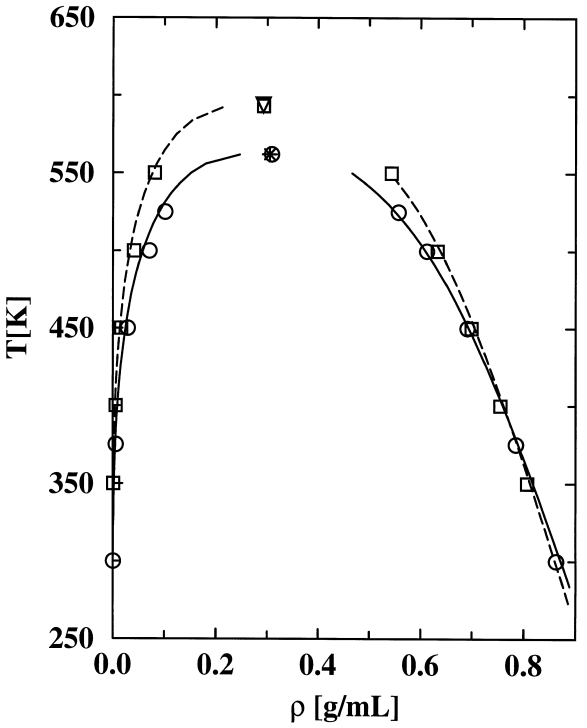

Fig. 1. Vapor–liquid coexistence curves for benzene and toluene, showing experimental densities [35] and critical points [45] for benzene (solid line and star, respectively) and toluene (dashed line and down triangle, respectively). Calculated densities and critical points are shown for benzene (circles) and toluene (squares). The statistical errors of the orthobaric densities are smaller than the symbol size.

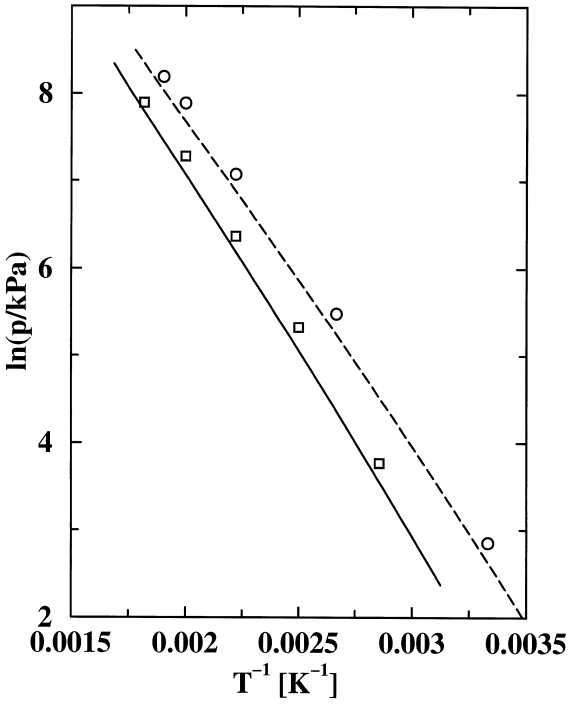

Fig. 2. Clausius–Clapeyron plots of saturated vapor pressure versus the inverse temperature. Experimental [35] and calculated data are shown for benzene (dashed line and circles, respectively) and toluene (solid line and squares, respectively). The statistical errors are smaller than the symbol size.

4. Simulation methods

Coupled–decoupled configurational-bias Monte Carlo simulations [15,30,31] in the constant-pressure Gibbs ensemble [33] were used to determine the gas–liquid partitioning for the model chromatographic system. The Gibbs ensemble uses multiple simulation boxes for the coexisting phases, that are kept in thermodynamic equilibrium via particle exchanges between boxes (phase equilibrium), via volume exchanges with a pressure bath (mechanical equilibrium), and particle displacements and conformational changes (thermal equilibrium). The stationary and mobile phases were represented by simulation boxes containing 96 squalane molecules and a total of 500 helium atoms, respectively. Whereas the helium carrier gas was allowed to swap between the two phases, the squalane molecules were always kept in the stationary phase box (the saturated vapor pressure is very low and an occasional squalane molecule in the mobile phase would not alter its properties to any significant extent). To maintain the infinite dilution limit for the analytes, only two analytes of each type (*n*-hexane, *n*-heptane, *n*-octane, benzene, and toluene) were included. The external pressure was set at 1 atm (1 atm = 101 325 Pa), and three separate sets of simulations were carried out at temperatures of 323, 353 and 383 K. For each temperature, ten independent simulations were carried out in parallel with a production period of 78 000 Monte Carlo (MC) cycles (one cycle consists of $N = 606$ moves) for each independent simulation. The statistical uncertainties reported are the standard errors of the mean determined from sets of independent simulations.

Table 2
Critical properties and normal boiling points calculated for the new and old [16] TraPPE–UA force fields and measured experimentally [45]. The subscripts denote the statistical uncertainties in the last digit of the simulation results

Molecule	T_c (K)			ρ_c (g/ml)			T_b (K)		
	New	Old	Exp.	New	Old	Exp.	New	Old	Exp.
Benzene	562_4	565_3	562_1	0.309_7	0.304_5	0.305_5	348_1	341_1	353.2
Toluene	593_5	594_4	594_2	0.293_7	0.298_7	0.292_2	376_2	370_1	383.8

The partition coefficients for the gas-to-liquid transfer of the analytes can be determined directly from the ratios of the average analyte number densities in the coexisting phases:

$$K_{\text{trans}} = \frac{\langle \rho_{\text{liquid}} \rangle}{\langle \rho_{\text{gas}} \rangle} = \exp[-\Delta G_{\text{trans}}/RT] \quad (7)$$

where R and T are the molar gas constant and absolute temperature, respectively. The number densities are mechanical properties, and hence the partition coefficients and Gibbs free energies of transfer can be determined more precisely following the Gibbs ensemble route [18–20] than using standard free energy evaluation techniques [37–39].

The Gibbs free energy of transfer can be separated into enthalpic and entropic contributions. The enthalpy of transfer itself contains two terms: the internal energy of transfer and the pressure-volume term. Assuming ideal mixing, the partial molar volume of any of the five solutes considered here is smaller than 200 ml mol^{-1}, hence the liquid part of the pressure-volume term is about 20 J mol^{-1}. The molar volume of the gas phase (very close to ideal since a helium carrier gas is used) can be determined directly from the simulations. The internal energy of transfer can also be evaluated directly from the simulations as follows:

$$\Delta U_{\text{trans}}^{\text{gas-liquid}} = \langle U_{\text{liquid}} \rangle - \langle U_{\text{gas}} \rangle \quad (8)$$

where U_{liquid} and U_{gas} are the internal energies of a given solute molecule (including intramolecular and intermolecular contributions), and these energies were calculated every ten MC cycles and averaged over the entire simulation. It should be noted that Eq. (8) assumes ideal solution behavior, i.e. that the internal energy of the solvent is not altered by the presence of the solute. Non-idealities should be small for the solute-solvent combinations investigated here. Since the enthalpy of transfer is calculated independently from the partition coefficients, the entropy of transfer at every specific temperature can be determined from the usual thermodynamic relation:

$$\Delta G(T) = \Delta H - T\,\Delta S \quad (9)$$

In chromatography experiments, absolute free energies are rarely measured, since the phase ratio is very difficult to determine, and varies significantly from column to column and also with temperature. Relative free energies, though, do not depend on the phase ratio, and are very reproducible [40].

5. Results and discussion

5.1. Gas chromatography experiments

All retention times measured are given in Table 3 and the retention indices of a number of aromatic molecules were determined as a function of temperature and are listed in Table 4. As shown in Fig. 3, these values compare very favorably (differences of less than 2 Kovats units) with previous measurements of the retention indices for these molecules [6,40–43]. Soják and Rijks [43] previously discussed the variations of Kovats retention indices for alkylbenzenes and showed that non-idealities of the carrier gases, differences in pressure drops, and ageing of the columns are the main factors contributing to the inter-laboratory variations. Finally, it should be noted that the peaks for *m*- and *p*-xylene at 373 and 383 K were not sufficiently separated in our chromatograms.

The measured retention indices for benzene, toluene and the xylenes increase with increasing temperature. The largest increase of about 17 units over the 60 K temperature range is observed for

Table 3
Experimental retention times

T (K)	Experimental retention time (min)									
	Void	Hexane	Heptane	Octane	Nonane	Benzene	Toulene	*p*-Xylene	*m*-Xylene	*o*-Xylene
323	1.230	1.958	3.184	6.429	14.952	2.275	4.227	9.485	9.663	11.293
333	1.231	1.767	2.598	4.682	9.880	2.004	3.328	6.703	6.813	7.853
343	1.231	1.636	2.214	3.594	6.870	1.817	2.738	4.969	5.038	5.722
353	1.232	1.543	1.956	2.895	5.025	1.685	2.340	3.856	3.901	4.363
363	1.233	1.477	1.779	2.435	3.860	1.588	2.066	3.121	3.149	3.471
373	1.233	1.427	1.652	2.121	3.099	1.518	1.872	2.629		2.870
383	1.233	1.389	1.560	1.902	2.589	1.463	1.731	2.281		2.454

o-xylene, and the smallest of about 14 units is found for *m*-xylene. The temperature dependence of the retention indices for all solutes is linear and the dI/dT values obtained from a linear regression are also listed in Table 4. With the exception of benzene, the dI/dT values agree very well with literature data [43].

5.2. Simulated gas–liquid partitioning

The calculated retention index, Gibbs free energies, enthalpies and entropies of transfer are summarized in Table 5. A graphical comparison of the calculated retention index to the experimental measurements of this work and to literature values [6,40–43] is shown in Fig. 3. The calculated retention indices for benzene are all higher than the experimental data measured in this work, and the root-mean-square deviation is 6 Kovats units. The root-mean-square deviation for toluene is 9 Kovats units, but the calculated values are substantially more scattered than those for benzene. The larger statistical uncertainties for toluene's retention index at the lower temperatures reflect the difficulty of swapping toluene and *n*-octane between the two phases at the lower temperatures and the fact that these two analytes partition more strongly into the stationary phase which leads to larger uncertainties in the average number densities in the vapor phase. Previous simulations for the old TraPPE–UA force field for benzene and toluene [21] yielded retention indices that were higher than experiment by 38 and 30 units, respectively. Thus, the addition of quadrupolar interactions leads to significant improvements for the predicted retention index for the new TraPPE–UA force field. In agreement with the experimental measurements, the calculated Kovats indices for benzene and toluene increase with in-

Table 4
Experimental retention indices

T(K)	Experimental retention index				
	Benzene	Toulene	*p*-Xylene	*m*-Xylene	*o*-Xylene
323	636.6	743.7	847.6	849.8	868.0
333	639.1	746.2	850.2	852.3	870.9
343	641.7	748.7	852.7	854.8	873.8
353	644.5	751.2	855.3	857.4	876.7
363	646.6	753.5	857.8	859.6	879.5
373	650.0	756.2	860.9		882.4
383	652.5	758.8	863.5		885.2
dI/dT	0.266	0.250	0.255[a]	0.247[a]	0.287
dI/dT[b]	0.240	0.245	0.251	0.245	0.284

[a] Calculated using only the data from 323 to 363 K.
[b] Taken from Ref. [43].

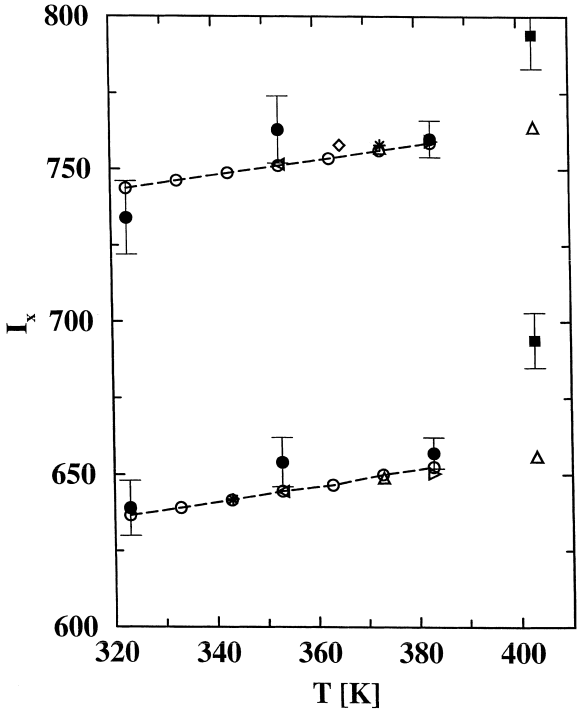

Fig. 3. Retention indices for benzene and toluene (sim.: filled circles; exptl.: open circles) at different temperatures. Simulation results for the previous model are depicted by filled squares. Literature experimental data are shown as stars [6], open diamonds [40], up triangles [41], right triangles [42], and left triangles [43].

creasing temperature. For the 60 K temperature range, the increases for benzene and toluene are 18 ± 10 and 26 ± 14 units.

The calculation of the enthalpic and entropic contributions to the Gibbs free energies of transfer allows us to rationalize the observed temperature dependence for the Kovats indices of the arenes. It is clearly evident from the values given in Table 5 that the entropies of transfer for the *n*-alkanes are significantly greater in magnitude than those for the arenes. This observation is consistent with previous studies of the solvation of *n*-alkanes and arenes in isotropic and oriented *n*-octadecane phases [44]. Using the standard thermodynamic equation for the Gibbs free energy given in Eq. (9), and assuming that the enthalpy and entropy are constant (see below), the temperature dependence of the Gibbs free energy is larger for molecules with larger entropies of transfer. This is the main reason why the Gibbs free energies of the *n*-alkanes increase at a greater rate than the arenes with increasing temperature, and the net effect is an increase in the relative Gibbs free energies of the arenes when compared to *n*-alkanes. Furthermore, this effect should lead to a linear temperature dependence of the retention index for the arenes, which is in good agreement with the measured data (see Fig. 3).

However, the calculated data clearly indicate that the assumption of constant enthalpies and entropies of transfer is a poor one for the vapor–liquid partitioning studied here. Both the enthalpy and the entropy of transfer decrease in magnitude with increasing temperature. These temperature dependencies can be rationalized by considering the thermal expansion of the liquid (or stationary) phase, i.e. the fact that the density of the liquid phase will decrease with increasing temperature. A decrease in the liquid density will lead to a corresponding decrease in the cohesive energy density which in turn lowers the internal energy (and enthalpy) for the vapor–liquid transfer, i.e. the enthalpy of transfer decreases with temperature (a fact that is well known for heats of vaporization). Furthermore, a decrease in the liquid density causes an increase in the free volume of the liquid phase and its compressibility. These factors lower the entropic cost of cavity formation. To quantify these arguments, the compressibility factors and Hildebrand solubility parameters of the stationary phase were calculated for the three temperatures (see Table 6). The calculated compressibility factors for the liquid phase show the expected increase, and the Hildebrand solubility parameters decrease by about 6% in good agreement with the observed changes in the internal energies and enthalpies of transfer.

6. Conclusions

Experimental measurements and molecular simulations show that the retention indices for benzene, toluene, and the three xylene isomers increase with increasing temperature by about 2–3 Kovats units per 10 K temperature increment. The molecular simulations allow for a direct determination of both the Gibbs free energy and the enthalpy of transfer,

Table 5
Partition coefficients and transfer properties

Solute	T (K)	I_x^{sim}	I_x^{exp}	ΔG_{trans} (kJ mol^{-1})	ΔH_{trans} (kJ mol^{-1})	ΔS_{trans} (kJ mol^{-1})
Benzene	323	639_9	637	-13.41_{14}	-27.86_7	-44.6_5
	353	654_8	645	-12.40_9	-27.14_5	-41.8_3
	383	657_5	652	-11.41_7	-26.47_4	-39.3_2
Toulene	323	734_{12}	744	-15.62_{20}	-32.00_9	-50.7_7
	353	763_{11}	751	-14.78_{15}	-31.14_8	-46.3_5
	383	760_6	759	-13.65_9	-30.27_7	-43.3_3
n-Hexane	323			-12.44_{15}	-32.35_8	-61.6_4
	353			-11.09_{13}	-31.47_7	-57.7_4
	383			-10.14_8	-30.50_9	-53.2_3
n-Heptane	323			-14.93_{13}	-36.84_9	-67.8_5
	353			-13.50_{13}	-35.62_8	-62.7_4
	383			-12.38_7	-34.39_8	-57.5_3
n-Octane	323			-16.99_{20}	-41.15_{12}	-74.8_7
	353			-15.55_7	-39.50_{11}	-67.8_4
	383			-14.48_{10}	-38.20_{11}	-61.9_4

The subscripts represent the uncertainties in the last digit(s).

and hence, the entropy of transfer can also be calculated using the standard thermodynamic relation. It is found that the alkane solutes exhibit larger (in magnitude) entropies of transfer than arenes with similar Gibbs free energies of transfer. Thus the Gibbs free energies of transfer for the alkane solutes increase more strongly with increasing temperature. It should also be noted that substantial temperature dependencies are observed for both the enthalpies and the entropies of transfer themselves which can be explained in terms of the temperature dependencies of the cohesive energy densities and the compressibility factors, respectively.

A new force field for alkylbenzenes is introduced that includes a 3-charge quadrupole in addition to Lennard–Jones sites for the CH(arom) and R–C(arom) groups. This force field yields small improvements for the vapor–liquid phase behavior of the neat arenes, but results in major improvements for alkane–arene mixture properties because the unlike dispersive interactions between these molecules are weakened for the new model compared to one that uses solely Lennard–Jones potentials for the arenes.

Table 6
Compressibility factors and Hildebrand solubility parameters

T (K)	κ (10^{-6} atm)	δ (J ml^{-1})
323	100_6	14.9_4
353	166_6	14.5_3
383	169_6	14.0_4

Acknowledgements

We thank Pete Carr for many stimulating discussions. Financial support from the National Science Foundation (CHE-9816328) and a Department of Energy Computational Science Graduate Fellowship (CDW) is gratefully acknowledged. Part of the computer resources were provided by the Minnesota Supercomputing Institute.

References

[1] H.M. McNair, E.J. Bonelli, Basic Gas Chromatography, Varian Instruments, Palo Alto, CA, 1968.
[2] G. Guiochon, C.L. Guillemin, Quantitative Gas Chromatography, Elsevier, Amsterdam, 1988.

[3] W. Jennings, E. Mittlefehldt, P. Stremple, Analytical Gas Chromatography, 2nd edition, Academic Press, San Diego, CA, 1997.
[4] E. Kovats, Helv. Chim. Acta 41 (1958) 1915.
[5] E. Kovats, Adv. Chromatogr. 1 (1965) 229.
[6] M.V. Budahegyi, E.R. Lombosi, T.S. Lombosi, S.Y. Mészáros, Sz. Nyiredy, G. Tarján, I. Timár, J.M. Takács, J. Chromatogr. 271 (1983) 213.
[7] J. Takács, M. Rockenbauer, I. Olácsi, J. Chromatogr. 42 (1969) 19.
[8] J. Takács, J. Chomatogr. A 799 (1998) 213.
[9] F.R. Gonzalez, A.M. Nardillo, J. Chromatogr. A 842 (1999) 29.
[10] E. Tudor, J. Chromatogr. A 858 (1999) 65.
[11] E. Tudor, J. Chromatogr. A 859 (1999) 49.
[12] J. Li, P.W. Carr, J. Chromatogr. A 670 (1994) 105.
[13] M.R. Schure, Adv. Chromatogr. 39 (1998) 139.
[14] M.G. Martin, J.I. Siepmann, J. Phys. Chem. B 102 (1998) 2569.
[15] M.G. Martin, J.I. Siepmann, J. Phys. Chem. B 103 (1999) 4508.
[16] C.D. Wick, M.G. Martin, J.L. Siepmann, J. Phys. Chem. B 104 (2000) 8008.
[17] G.C. Maitland, M. Rigby, E.B. Smith, W.A. Wakeham, Intermolecular Forces: Their Origin and Determination, Clarendon Press, Oxford, 1981.
[18] M.G. Martin, J.I. Siepmann, J. Am. Chem. Soc. 119 (1997) 8921.
[19] M.G. Martin, J.I. Siepmann, Theo. Chem. Acc. 99 (1998) 347.
[20] M.G. Martin, J.I. Siepmann, M.R. Schure, J. Phys. Chem. B 103 (1999) 11191.
[21] C.D. Wick, M.G. Martin, J.I. Siepmann, M.R. Schure, Int. J. Thermophys. 22 (2001) 111.
[22] J.J. Potoff, J.I. Siepmann, AIChE J. 47 (2001) 1676.
[23] S.T. Howard, T.M. Krygowski, Can. J. Chem. 75 (1997) 174.
[24] D.R. Lide (Ed.), CRC Handbook of Chemistry and Physics, 72nd edition, CRC Press, Boca Raton, FL, 1991.
[25] M. Claessens, M. Ferrario, J.P. Ryckaert, Mol. Phys. 50 (1983) 217.
[26] M.P. Allen, D.J. Tildesley, Computer Simulation of Liquids, Oxford University Press, Oxford, 1987.
[27] K.B. Lipkowitz, M.A. Peterson, J. Comput. Chem. 14 (1993) 121.
[28] J.M. Takács, J. Chromatogr. Sci. 29 (1991) 382.
[29] R.T. Sanderson, Chemical Bonds and Bond Energies, Academic Press, New York, 1971.
[30] J.I. Siepmann, D. Frenkel, Mol. Phys. 75 (1992) 59.
[31] D. Frenkel, G.C.A.M. Mooji, B. Smit, J. Phys. Condens. Matter. 4 (1992) 3053.
[32] A.Z. Panagiotopoulos, Mol. Phys. 61 (1987) 813.
[33] A.Z. Panagiotopoulos, N. Quirke, M. Stapleton, D.J. Tildesley, Mol. Phys. 63 (1988) 527.
[34] B. Smit, P. de Smedt, D. Frenkel, Mol. Phys. 68 (1989) 931.
[35] B.D. Smith, R. Srivastava, Thermodynamic Data for Pure Compounds: Part A, Hydrocarbons and Ketones, Elsevier, Amsterdam, 1986.
[36] B. Chen, J.I. Siepmann, J. Phys. Chem. B 103 (1999) 5370.
[37] W.L. Jorgensen, Acc. Chem. Res. 22 (1989) 184.
[38] P.A. Kollman, Acc. Chem. Res. 29 (1996) 461.
[39] R.J. Radmer, P.A. Kollman, J. Comput. Chem. 18 (1997) 902.
[40] J. Krupcik, O. Liska, L. Soják, J. Chromatogr. 51 (1970) 119.
[41] L.E. Cook, F.M. Raushel, J. Chromatogr. 65 (1972) 556.
[42] D.I. Papazova, M.C. Pankova, J. Chromatogr. 105 (1975) 411.
[43] L. Soják, J.A. Rijks, J. Chromatogr. 119 (1976) 505.
[44] C.D. Wick, J.I. Siepmann, M.R. Schure, J. Phys. Chem. B 105 (2001) 10961.
[45] NIST WebBook, http://webbook.nist.gov/chemistry/